Dual Level Direct ab Initio and Density-Functional Theory Dynamics Study on the Unimolecular Decomposition of CH_3OCH_2 Radical

Qian Shu Li,*,†,‡ Yue Zhang,†,§ and Shaowen Zhang*,†

School of Science, Beijing Institute of Technology, Beijing 100081, P. R. China, Institute of Theoretical Chemistry, State Key Laboratory of Theoretical and Computational Chemistry, Jilin University, Changchun 130023, P. R. China, and Department of Chemistry, Shijiazhuang Normal College, Shijiazhuang 050801, P. R. China

Received: October 18, 2003; In Final Form: December 19, 2003

We presented a direct ab initio and density-functional theory dynamics study of the thermal rate constants of the unimolecular decomposition reaction of $CH_3OCH_2 \rightarrow CH_2O + CH_3$ at a wide temperature range of 200−2500 K. MPW1K/6-31+G(d,p), MP2/6-31+G(d,p), and QCISD/6-31+G(d,p) methods were employed to optimize the geometries of all stationary points and to calculate the minimum energy path (MEP). The energies of all the stationary points were refined at the QCISD(T)/aug-cc-pVTZ level of theory. The rate constants were evaluated based on the energetics from the QCISD(T)/aug-cc-pVTZ//MPW1K/6-31+G(d,p) level of theory using both microcanonical variational transition state theory (μVT) and canonical variational transition state theory (CVT) in the temperature range of 200−2500 K. The calculated rate constants at the QCISD(T)/aug-cc-pVTZ//MPW1K/6-31+G(d,p) level of theory are in good agreement with experimental data. The fitted three-parameter Arrhenius expression from the μVT rate constants in the temperature range 200−2500 K is $k = 4.45 \times 10^{14} T^{-0.22}\ e^{(-1.37\times10^4/T)}\ s^{-1}$.

1. Introduction

Ethers and ether derivatives are important species in a variety of chemical processes involved in atmospheric and combustion chemistry.[1−3] For example, ether derivatives such as methyl *tert*-butyl ether (MTBE) are used as fuel additives to reduce engine knocking.[4] Although most of ethers and ether derivatives would be consumed in the combustion process, some fraction will reach the environment from incomplete combustion and from losses during fueling. As a result, it is important to ascertain the environmental impact of their emissions. Also, understanding the atmospheric oxidation process is paramount to developing solutions to minimize pollution from their emissions. Dimethyl ether (DME), one of the simplest ethers from the branched aliphatic ether family, is believed to be a cleaner in the combustion process and, as a consequence, is being considered as a replacement for diesel fuel. It has a number of desirable properties[5] that make it an attractive diesel fuel. Once released in the atmosphere, dimethyl ether is degraded by a reaction with tropospheric hydroxyl radical.[6] This reaction produces CH_3OCH_2 radicals, that is,

$$CH_3OCH_3 + OH \rightarrow CH_3OCH_2 + H_2O$$

The subsequent atmospheric fate and the environmental impact of dimethyl ether emissions will depend on how the CH_3OCH_2 radical participates in further degradation in the atmosphere. Because of the significance in atmospheric and combustion chemistry, the unimolecular decomposition reaction of CH_3OCH_2 radical, which yields stable formaldehyde and methyl radical, has been widely studied by many researchers[5,7−11]. Dagaut et al.[8] studied the combustion of DME in a jet-stirred reactor at temperatures of 850−1300 K and pressures of 1−10 bar followed by detailed kinetic modeling of the obtained experimental data. They drew a conclusion that the unimolecular decomposition reaction was the dominant fate of CH_3OCH_2 radicals at combustion temperatures. Loucks and Laidler[9] obtained the reaction rate constant of $k = 1.6 \times 10^{13}\ e^{-25.44(kcal\cdot mol^{-1})}\ s^{-1}$ in the temperature range from 373 to 473 K and at pressures of 0−0.8 bar by means of sensitized photolysis and gas chromatography techniques. Sehested et al.[7] measured the reaction rate constant using pulse radiolysis coupled with time-resolved UV absorption spectroscopy. The decay rate of CH_3OCH_2 radicals was $k = 1.6 \times 10^{13}\ e^{-25.44(kcal\cdot mol^{-1})}\ s^{-1}$ in the temperature range of 573−666 K at 18 bar total pressure. It is evident that the rate constant of CH_3OCH_2 radical unimolecular decomposition determined from Sehested et al. is consistent with that from Loucks and Laidler. Regretfully, the decay rates of the CH_3OCH_2 radical obtained from either Loucks and Laidler or Sehested et al. were determined over a narrow temperature range. In addition, it should be mentioned that the title reaction is expected to be the most important loss reaction for CH_3OCH_2 radical at combustion temperatures above 1000 K. To provide detailed information regarding the underlying mechanism and acquire accurate thermal rate constants over a wide temperature range, high-level ab initio calculation and rate constants calculation are still required.

In the present study, the potential energy surface (PES) was constructed from DFT and ab initio methods, and the gas-phase thermal rate constants for the reactions of $CH_3OCH_2 \rightarrow CH_2O + CH_3$ were calculated using the microcanonical variational transition state theory[12,13] (μVT) and canonical variational transition state theory (CVT) based on the direct ab initio dynamics approaches.[14,15]

* Author to whom correspondence should be addressed. Phone: +86-10-68912665. Fax: +86-10-68912665. E-mail: qsli@bit.edu.en.
† Beijing Institute of Technology.
‡ State Key Laboratory of Theoretical and Computational Chemistry.
§ Shijiazhuang Normal College.

10.1021/jp037154w CCC: $27.50
Published on Web 02/20/2004

2. Methodology

2.A. Electronic Structure Calculations. It has been shown that the hybrid Hartree−Fock density-functional method, abbreviated HDFT, and in particular, MPW1K, provides a good alternative for a wide variety of applications in kinetics.[16] Here MPW1K denotes a new DFT model proposed by Truhlar and co-workers,[16] which is called the modified Perdew−Wang 1-parameter model for kinetics. The QCISD(T) method can provide quite reasonable energetics for this type of reaction.[17] QCISD(T) is referred to as the quadratic CI calculation including single and double substitutions with a triples contribution to the energy added.[18] Combining the MPW1K geometries with QCISD(T) single-point energy refinement, that is, the dual level electronic structure calculations QCISD(T)//MPW1K, will give reasonable potential energy information.[19] Furthermore, the MPW1K method is quite accurate for saddle point geometries, and the successful use of the method for calculating geometries in conjunction with single-point calculations at the QCISD(T) and CCSD(T) levels of theory would achieve a reasonable potential energy surface.[19,20] Another computational advantage of the MPW1K method would allow the application of the direct dynamics method in the study of reactions involving large polyatomic molecules. For comparison, in addition to the MPW1K/6-31+G(d,p) method, the geometric parameters, gradients, and Hessians of all the stationary points for the title reactions were computed at the MP2/6-31+G(d,p) and QCISD/6-31+G(d,p) levels of theory. To confirm the connection between a transition state (TS) and given reactants and products, the minimum energy paths (MEPs) were calculated using the intrinsic reaction coordinate (IRC) method[21] in mass-weighted Cartesian coordinates with a step size of 0.01 $(amu)^{1/2}$ bohr at the MPW1K/6-31+G(d,p) level of theory. The generalized harmonic vibrational frequencies of selected points along the MEP were also calculated at the same level of theory. The single-point energies of all the stationary points were refined at the QCISD(T)/aug-cc-pVTZ//MPW1K/6-31+G(d,p) level of theory to obtain more reliable energetics. cc-pVTZ and aug-cc-pVTZ is Dunning's correlation consistent polarized valence triple-ζ basis set without and with the augmentation of diffuse function.[22] To construct an accurate potential energy profile, the QCISD(T)/aug-cc-pVTZ method was employed to refine the energies of points along the MEP optimized at the MPW1K/6-31+G(d,p) level of theory. For convenience, we denote the QCISD(T)/aug-cc-pVTZ//MPW1K/6-31+G(d,p) method as QCISD(T)//MPW1K. All the above calculations were performed using the Gaussian 98 program suite.[23]

2.B. Rate Constant Calculations. The variational transition state rate constant for a gas-phase reaction is determined by varying the location of the dividing surface along a reference path to minimize the rate constant at a given temperature, thus keeping a possibility to minimize the error due to "recrossing" trajectories.[24−26] In the present study, the reference path is the minimum energy path (MEP) that is defined as the steepest descent path from the saddle point to both the reactant and product sides in the mass-weighted Cartesian coordinate system. The reaction coordinate, s, is defined as the distance along the MEP with the origin located at the saddle point and is positive on the product side and negative on the reactant side. For a canonical ensemble at a given temperature T, the canonical variational transition state theory (CVT) thermal rate constant $k^{CVT}(T)$ is given by

$$k^{CVT}(T) = \min_s k^{GT}(T,s)$$

where $k^{GT}(T,s)$ is the generalized transition state theory rate constant at the dividing surface which intersects the MEP at s and is orthogonal to the MEP at the intersection point.

$$k^{GT}(T,s) = \left\{ \sigma \frac{k_B T}{h} \frac{Q^{GT}(T,s)}{\Phi^R(T)} e^{-V_{MEP}(s)/k_B T} \right\}$$

Here, k_B is Boltzmann's constant and h is Planck's constant; σ is the symmetry factor accounting for the possibility of more than one symmetry-related reaction path and can be calculated as the ratio of the product of the reactant rotational symmetry numbers to that of the transition state. For the present case, we adopt the symmetry factor of 1 in the calculation of rate constants because of the fact that only one reaction channel is found connecting the reactants and products as the carbon atom and oxygen break. Q^{GT} is the internal partition function of the generalized transition state with the local zero of energy at $V_{MEP}(s)$, which is the classical potential energy along the minimum energy path with its zero of energy at the reactants. Φ^R is the reactant partition function per unit volume for bimolecular reactions. Both the Q^{GT} and Φ^R are approximated as products of electronic, rotational, and vibrational partition functions. For Φ^R, the relative translational partition function is also included. The translational and rotational partition functions are evaluated classically, whereas the vibrational partition functions are calculated quantum mechanically within the harmonic approximation for the present studies.

The microcanonical variational transition state theory (μVT)[13,27,28] is based on the idea that by minimizing the microcanonical rate constants $k(E)$ along the MEP, one can minimize the error caused by the "recrossing" trajectories. Within the framework of μVT, the rate constant at a fixed temperature T can be expressed as

$$k^{\mu VT}(T) = \frac{\int_0^\infty \min\{ N^{GTS}(E,s)\} e^{-E/k_B T} dE}{hQ^R}$$

where Q^R is the total reactant partition function, which is the product of the electronic, rotational, and vibrational partition functions. The relative translational partition function was calculated classically and is included in Q^R. However, the rotational and vibrational partition functions of the reactant were calculated quantum mechanically within the rigid rotor and harmonic oscillator approximations, respectively. $N^{GTS}(E,s)$ is the sum of states of electronic, rotational, and vibrational motions at energy E of the generalized transition state located at s, where s is the reaction coordinate. $N^{GTS}(E,s)$ along the MEP was also calculated quantum mechanically using the rigid rotor and harmonic oscillator approximations. In addition, because the reaction involves a scission between heavy atoms (C−O), the tunneling effect is expected to be small. Thus, the tunneling effect is not considered in the present study.

The gas-phase thermal rate constants of the title reaction are calculated using the above two levels of theory, namely, the microcanonical variational transition state theory (μVT) and canonical variational transition state theory (CVT). All rate constants were calculated employing the online Vklab program.[29]

3. Results and Discussion

3.A. Stationary Points. Pictorial diagrams of optimized geometries of the stationary points are shown in Figure 1. Table 1 lists the optimized geometric parameters of the equilibrium

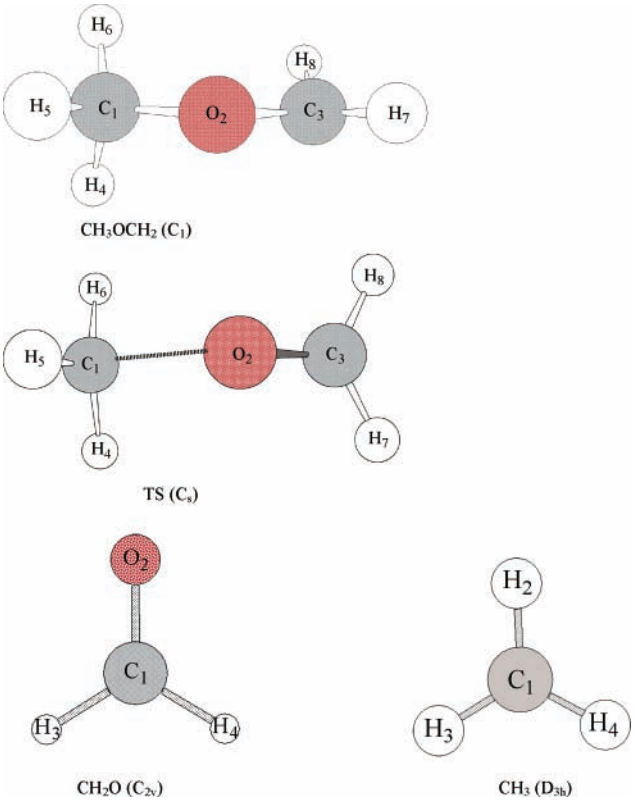

Figure 1. Pictorial diagram of optimized geometries of the stationary points.

and transition state at the MPW1K/6-31+G(d,p), MP2/6-31+G(d,p), and QCISD/6-31+G(d,p) levels of theory along with the available experimental and theoretical data.[30−33] For the stable species, it can be seen that both bond lengths and bond angles predicted at these levels of theory are in good agreement with one another as well as with the experimental and theoretical data. Moreover, both bond lengths and bond angles of CH_2O predicted at the MPW1K/6-31+G(d,p) level of theory are closer to the available experimental data and the RCCSD(T)/TZ2P(f,d) theoretical prediction[31] than those at the MP2/6-31+G(d,p) level of theory. It is worth noting that the predicted C_1-O_2 and O_2-C_3 bond lengths of the CH_3OCH_2 radical at the MPW1K/6-31+G(d,p) level of theory are slightly short compared to those at the other, MP2/6-31+G(d,p) and QCISD/6-31+G(d,p), levels of theory; meanwhile, the other bond lengths and bond angles are quite close to one another at the three levels of theory. For the transition states, the breaking bond distances (C_1-O_2) are 1.948Å, 1.921Å, and 1.926Å at the MPW1K/6-31+G(d,p), MP2/6-31+G(d,p), and QCISD/6-31+G(d,p) levels of theory, respectively. The breaking bond lengths (C_1-O_2) at the MPW1K/6-31+G(d,p) level of theory are about 0.027Å and 0.021Å slightly longer than those at the MP2/6-31+G(d,p) and QCISD/6-31+G(d,p) levels of theory, respectively. The breaking bond length (C_1-O_2) increases by about 0.5Å compared to that of the reactant CH_3OCH_2 radical at the three levels of theory, respectively. The forming bond lengths (O_2-C_3) are 1.245, 1.237, and 1.273Å at the MPW1K/6-31+G(d,p), MP2/6-31+G(d,p), and QCISD/6-31+G(d,p) levels of theory, respectively, which are about 0.1Å shorter than that of the reactant CH_3OCH_2 radical at the level of theory.

Table 2 lists the harmonic vibrational frequencies and zero-point energies of reactants, transition states, and products using MPW1K, MP2, and QCISD methods using the same 6-31+G(d,p) basis set along with the available experimental data.[34−38] For the stationary points, the calculated frequencies at the three

TABLE 1: Optimized Geometries of Reactant and Products from the MPW1K, MP2, and QCISD Methods Using the Same 6-31+G(d,p) Basis Set[a]

species		MPW1K	MP2	QCISD	ref
CH_3OCH_2 (C_1)	R(1,2)	1.402	1.429	1.428	
	R(1,5)	1.084	1.085	1.087	
	R(1,4;6)	1.092	1.092	1.093	
	R(2,3)	1.343	1.364	1.368	
	R(3,7)	1.076	1.077	1.079	
	R(3,8)	1.082	1.084	1.085	
	A(2,1,5)	107.2	106.4	106.5	
	A(2,1,4;6)	110.9	110.3	110.4	
	A(4,1,5)	109.5	110.1	110.0	
	A(4,1,6)	109.2	109.7	109.7	
	A(5,1,6)	109.3	109.8	109.8	
	A(1,2,3)	115.2	113.7	113.9	
	A(2,3,7)	113.8	112.7	112.9	
	A(2,3,8)	118.2	117.3	117.4	
	A(7,3,8)	121.3	120.5	120.5	
CH_2O (C_{2v})	R(1,2)	1.196	1.224	1.219	1.209[b], 1.203[c]
	R(1,3;4)	1.100	1.099	1.100	1.113[b], 1.099[c]
	A(2,1,3)	121.8	121.7	121.8	121.8[b], 121.8[c]
	A(3,1,4)	116.5	116.5	116.4	116.4[b], 116.5[c]
CH_3 (D_{3h})	R(1,2)	1.076	1.075	1.078	
TS (C_s)	R(1,2)	1.948	1.921	1.926	
	R(1,4)	1.077	1.078	1.080	
	R(1,5)	1.078	1.079	1.082	
	R(1,6)	1.078	1.079	1.082	
	R(2,3)	1.245	1.237	1.273	
	R(3,7)	1.092	1.094	1.092	
	R(3,8)	1.092	1.094	1.092	
	A(4,1,5)	117.0	116.8	116.5	
	A(4,1,6)	117.0	116.8	116.5	
	A(5,1,6)	117.4	117.0	116.7	
	A(1,2,3)	119.0	120.8	117.5	
	A(2,3,7;8)	120.9	121.4	120.7	
	A(7,3,8)	118.0	117.1	118.4	

[a] Note that, for the numbers (refer to Figure 1) with the semicolon, both sides in the parenthesis are identical. Bond lengths (R) in angstroms and bond angles (A) in degrees. [b] From theoretical prediction at the RCCSD(T)/TZ2P(f,d) level of theory (see ref 31). [c] References 32 and 33.

levels of theory are generally in good agreement with the corresponding experimental values[34−38] except that the frequencies of CH_3 have some deviation from literature values. However, one can see that the discrepancy between the theoretical results and experimental data are generally within 5% except for the lowest frequency of the CH_3 radical. For the transition states, the frequencies predicted from the MPW1K/6-31+G(d,p), MP2/6-31+G(d,p), and QCISD/6-31+G(d,p) levels of theory are consistent with each other. In particular, the predicted values of the imaginary frequency are 658, 1146, and 833 cm^{-1} at the MPW1K/6-31+G(d,p), MP2/6-31+G(d,p), and QCISD/6-31+G(d,p) levels of theory, respectively. For every stationary point, the zero-point energies are close to one another at the three different levels of theory.

The reaction energetics information including the reaction energies (ΔE), the reaction enthalpies (ΔH^0_{298K}), and the classical potential barriers ($V^{\neq}$) calculated at different levels of theory are listed in Table 3 along with the available experimental data[6,7,39]. As can be seen from Table 3, the predicted reaction enthalpies (298K) for the reaction at the MPW1K/6-31+G(d,p), PMP2/6-31+G(d,p) and QCISD/6-31+G(d,p) levels of theory are 12.94, 4.98, and 3.23 kcal mol^{-1}, respectively, which deviate more or less from the experimental value of 7.80 kcal mol^{-1}.[6,39] Subsequently, to obtain reliable energetics information that play a crucial role in the rate constant calculations, the single-point energy calculations are improved based on MPW1K-optimized

TABLE 2: Harmonic Vibrational Frequencies (cm^{-1}) and Zero-Point Energies (kcal mol^{-1}) of Reactant, Products, and the Transition State from the MPW1K, MP2, and QCISD Methods Using the Same 6-31+G(d,p) Basis Set

species	method	frequencies	ZPE[a]
CH_3OCH_2 (C_1)	MPW1K	173, 295, 437, 618, 1031, 1171, 1208, 1295, 1363, 1499, 1532, 1541, 1549, 3097, 3172, 3209, 3243, 3367	42.60
	Mp2	169, 314, 437, 752, 978, 1160, 1193, 1277, 1301, 1499, 1536, 1541, 1553, 3105, 3194.3401, 3205, 3260, 3372	42.67
	QCISD	168, 304, 438, 730, 979, 1155, 1193, 1278, 1300, 1498, 1533, 1538, 1551, 3084, 3160, 3179, 3225, 3333	42.38
CH_2O (C_{2v})	MPW1K	1241, 1299, 1577, 1914, 3021, 3097	17.37
	MP2	1211, 1282, 1569, 1760, 3039, 3123	17.13
	QCISD	1207, 1286, 1571, 1799, 3020, 3095	17.13
exptl[b]		1167, 1249, 1500, 1746, 2783, 2843	
CH_3 (D_{3h})	MPW1K	520, 1443, 1443, 3210, 3402, 3402	19.19
	MP2	467, 1478, 1478, 3234, 3432, 3432	19.33
	QCISD	485, 1465, 1465, 3186, 3373, 3373	19.08
exptl[c]		603, 1403, 3004, 3171	
TS (C_s)	MPW1K	88, 265, 294, 653, 677, 965, 991, 1253, 1399, 1461, 1467, 1601, 3090, 3188, 3196, 3370, 3382, 658*i*	39.09
	MP2	93, 287, 294, 684, 705, 1003, 1092, 1269, 1375, 1489, 1491, 1620, 3083, 3181, 3201, 3382, 3396, 1146*i*	39.52
	QCISD	93, 198, 291, 662, 696, 916, 1018, 1234, 1302, 1482, 1484, 1590, 3089, 3162, 3189, 3326, 3341, 833*i*	38.70

[a] ZPE in the last column denotes the zero-point energy. [b] Reference 35. [c] References 36−38.

TABLE 3: Reaction Energetics Parameters (kcal mol^{-1}) at Various Levels of Theory

method	ΔE^a	ΔH^0_{298K}	$V^{\neq}$ [b]
MPW1K/6-31+G(d,p)	11.39	12.94	28.87
PMP2/6-31+G(d,p)	3.30	4.98	26.60
QCISD/6-31+G(d,p)	1.64	3.23	25.90
QCISD(T)/cc-pVTZ//MPW1K/6-31+G(d,p)	6.60	8.15	25.50
exptl		7.8[c]	25.44[d]

[a] Reaction energy with zero-point energy correction. [b] The classical potential barrier with zero-point energy correction. [c] References 6 and 39. [d] References 7 and 9.

geometries. The refined reaction enthalpies are 8.15 kcal mol^{-1} at the QCISD(T)/aug-cc-pVTZ//MPW1K/6-31+G(d,p) level of theory, which is the closer to the experimental value of 7.80 kcal mol^{-1} than those from the MPW1K/6-31+G(d,p), PMP2/6-31+G(d,p), and QCISD/6-31+G(d,p) levels of theory. Thus, the QCISD(T) method with an augmentation of diffuse functions to the aug-cc-pVTZ basis set can substantially improve the reaction enthalpy. In particular, the geometries optimized at the MPW1K/6-31+G(d,p) level of theory seem more reasonable compared to the available experimental values in the present study. The zero-point-energy-corrected classical potential barriers are 28.87, 26.60, 25.90, and 25.50 kcal mol^{-1} at the MPW1K/6-31+G(d,p), PMP2/6-31+G(d,p), QCISD/6-31+G(d,p), and QCISD(T)/aug-cc-pVTZ//MPW1K/6-31+G(d,p) levels of theory, respectively. Again, the barrier heights (25.50 kcal mol^{-1}) calculated using QCISD(T) are in excellent agreement with the experimental data (25.44 kcal mol^{-1}).[7,9] The barrier heights predicted from the PMP2 and QCISD methods are closer to the experimental data than that predicted from the MPW1K method. In contrast, of all the methods, the QCISD(T) method gives the best theoretical prediction from the viewpoint of energetics. This implies that the reaction energetics can be effectively improved by the QCISD(T) methods with the aug-cc-pVTZ basis set for the present reaction. Because the MPW1K method provides reasonable geometries of saddle points and the QCISD(T) method gives good energetics predictions,[16,19,20] the energies, geometries, gradients, and Hessians of the selected points along the MEP are obtained by the dual level QCISD(T)//MPW1K method.

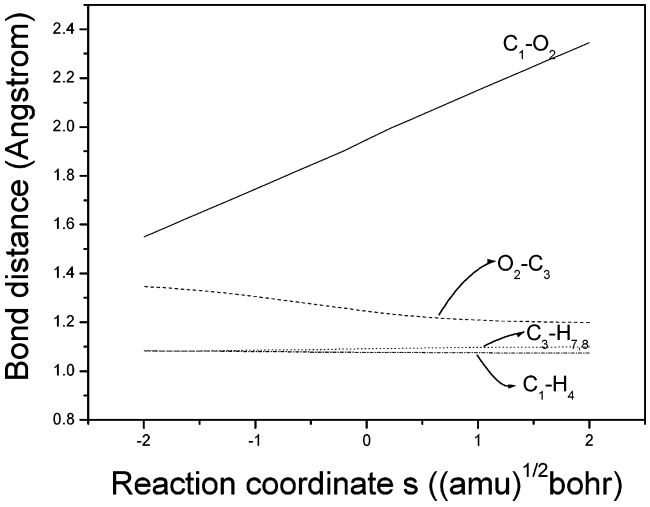

Figure 2. Variations of selected bond lengths along the minimum energy path of the unimolecular decomposition as a function of reaction coordinate *s* ((amu)$^{1/2}$ bohr) at the MPW1K/6-31+G(d,p) level of theory. The solid line denotes the breaking C_1-O_2 bond length; the dashed line denotes the forming O_2-C_3 bond length; the dotted line denotes the $C_3-H_{7,8}$ bond length; the dash-dot-dash line denotes the C_1-H_4 bond length.

3.B. Reaction Path Properties. The mass-weighed minimum energy paths[40] were obtained using the intrinsic reaction coordinate (IRC) algorithm[21] at the MPW1K/6-31+G(d,p) level of theory, and the potential energy profiles were further refined at the QCISD(T)/aug-cc-pVTZ level of theory. Figure 2 shows the variation of the selected C−O and C−H bond lengths along the minimum energy path of the unimolecular decomposition as a function of reaction coordinate *s* ((amu)$^{1/2}$ bohr) at the MPW1K/6-31+G(d,p) level of theory. In the course of the reaction, the breaking C_1-O_2 bond length almost linearly increases, while the forming O_2-C_3 bond length of the CH_2O molecule gradually shortens from $s = -2$ (amu)$^{1/2}$bohr to $s = 2$ (amu)$^{1/2}$bohr. The $C_3-H_{7,8}$ bond lengths slightly increase and the C_1-H_4 bond length is almost unchanged during the reaction process.

Figure 3 presents the classical potential energy (V_{MEP}) and vibrationally adiabatic ground-state potential energy (V_a^G) curves of the reaction as a function of reaction coordinate *s* ((amu)$^{1/2}$ bohr) at the QCISD(T)/aug-cc-pVTZ//MPW1K/6-31+G(d,p) level of theory. As can be seen, the position of the maximum of the $V_{MEP}(s)$ and the $V_a^G(s)$ energy curves is the same and the two curves are very similar in shape. The $V_{MEP}(s)$ curve is flat around the transition state. Thus, we adopt the variational method to calculate the thermal gas-phase rate constants in the μVT and CVT framework. However, because the reaction involves a scission between heavy atoms (C−O), the tunneling effect is expected to be small. Thus, the tunneling effect will not be considered here.

3.C. Rate Constant Calculations. The thermal gas-phase rate constants of the reaction are calculated using the microcanonical variational transition state theory (μVT) and canonical variational transition state theory (CVT) employing the MEP calculated at the QCISD(T)/aug-cc-pVTZ//MPW1K/6-31+G(d,p) level of theory within the temperature range of 200−2500

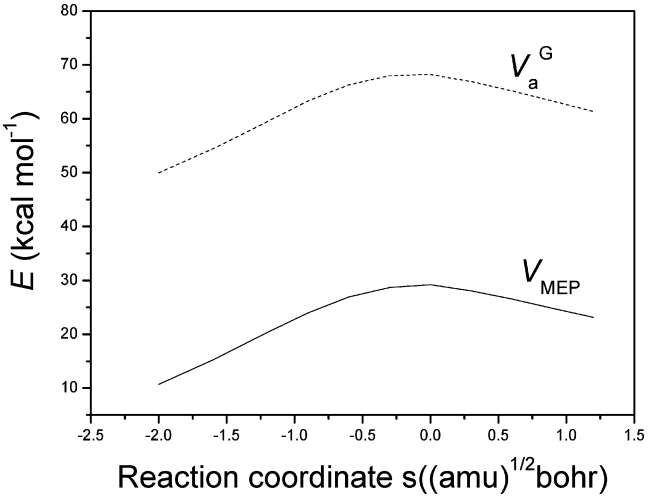

Figure 3. The classical potential energy (V_{MEP}) and vibrationally adiabatic ground-state potential energy (V_a^G) curves of the reaction as a function of reaction coordinate s ((amu)$^{1/2}$ bohr) at the QCISD(T)/aug-cc-pVTZ//MPW1K/6-31+G(d,p) level of theory. The solid line denotes the V_{MEP} curve; the dashed line denotes the V_a^G curve.

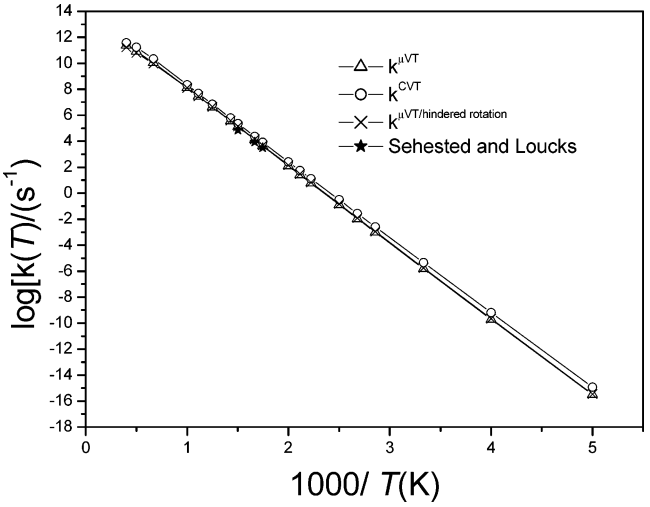

Figure 4. Comparison between the calculated forward rate constants at the QCISD(T)/aug-cc-pVTZ//MPW1K/6-31+G(d,p) level of theory and the available experimental data. $k^{\mu VT/hindered\ rotation}$ denotes the rate constant including the hindered rotation.

K. The calculated forward rate constants are shown in Figure 4, together with available experimental data.[7,9] It can be seen from Figure 4 that the forward rate constants show positive temperature dependence in the temperature range of 200−2500 K, which agrees very well with the recent measurement from Sehested et al. For example, at 573 K the μVT and CVT rate constants are 4.3×10^3 s^{-1} and 8.1×10^3 s^{-1}, which are close to the experimental rate constant $k = 3.2 \times 10^3$ s^{-1} obtained by Sehested and Loucks.[7,9] At 666 K the μVT and CVT rate constants are 1.3×10^5 s^{-1} and 2.2×10^5 s^{-1}, which are close to the experimental rate constant $k = 7.2 \times 10^4$ s^{-1} obtained by Sehested et al..[7,9] The predicted values of μVT rate constants, whether at low temperature or at high temperature, are closer to the recent measured values[7,9]than the CVT rate constants in the experimental measurement temperature range of 573−666 K. The experimental results are consistently smaller than the theoretical μVT and CVT rate constants in the experimental measurement temperature, which is in keeping with the principle of the variational transition state theory,[41] $k^{TST}(T) > k^{CVT}(T) > k^{\mu VT}(T) > k_c^0$. The hindered rotation of the methyl group in the TS region could be important to the rate of this reaction in the high-temperature range. The μVT rate constants including the hindered rotation effect were also calculated and plotted in Figure 4. It is obvious that the μVT rate constants including the hindered rotation are very close to the μVT rate constants in the calculated temperature range, with the deviations being a factor of 1.10 and 1.07 at 573 and 666 K, respectively. The μVT rate constants of this reaction including the hindered rotation are slightly smaller than the μVT rate constants without hindered rotation when the temperature is above 900 K. Furthermore, the forward μVT rate constants within the temperature range of 200−2500 K are fitted to the three-parameter Arrhenius expression in units of s^{-1} as follows:

$$k = 4.45 \times 10^{14} T^{-0.22}\, e^{(-1.37\times 10^4/T)}$$

4. Summary

We presented a direct ab initio dynamics study of the thermal rate constants of the unimolecular decomposition reaction of $CH_3OCH_2 \rightarrow CH_2O + CH_3$. The MPW1K/6-31+G(d,p), MP2/6-31+G(d,p), and QCISD/6-31+G(d,p) methods were employed to optimize the geometries of stationary points. The minimum energy path was computed at the MPW1K/6-31+G(d,p) level of theory. The single-point energies of all the stationary points were refined at the QCISD(T)/aug-cc-pVTZ//MPW1K/6-31+G-(d,p) levels of theory. For the present system studied, the geometric parameters, harmonic vibrational frequencies, and energetics information from the dual level method was reliable compared to the available experimental data. The thermal rate constants were evaluated based on the electronic structure and energy information from the QCISD(T)/aug-cc-pVTZ//MPW1K/6-31+G(d,p) level of theory with both microcanonical variational transition state theory (μVT) and canonical variational transition state theory (CVT) in the temperature range of 200−2500 K. The theoretical results showed that the calculated forward rate constants at the QCISD(T)/aug-cc-pVTZ//MPW1K/6-31+G(d,p) level of theory at the measured temperature region were in excellent agreement with available experimental data and have a positive temperature dependence in the calculated temperature ranges. The fitted Arrhenius expression from the forward μVT rate constants within the temperature range of 200−2500 K is $k = 4.45 \times 10^{14}\ T^{-0.22}\ e^{(-1.37\times 10^4/T)}$ s^{-1}. It is anticipated that the calculated results will be very useful for ascertaining the environmental impact of CH_3OCH_2 radical and understanding the atmospheric oxidation process that is important in the development of solutions to minimize pollution from their emissions.

Acknowledgment. This work was supported by the National Natural Science Foundation of China (20373007) and the Foundation for basic research by the Beijing Institute of Technology.

References and Notes

(1) Wallington, T. J.; Dagaut, P.; Liu, R.; Kurylo, M. J. *Environ. Sci. Technol.* **1988**, *22*, 842.

(2) Demore, W. B.; Hsu, K. J. *J. Phys. Chem.* **1995**, *99*, 11141.

(3) Wrobel, R.; Sander, W.; Kraka, E.; Cremer, D. *J. Phys. Chem. A* **1999**, *103*, 3693.

(4) Smith, D. F.; Kleindienst, T. E.; Hydgens, E. E.; McIver, C. D. *Int. J. Chem. Kinet.* **1991**, *23*, 907.

(5) Yamada, T.; Bozzelli, J. W.; Lay, T. H. *Int. J. Chem. Kinet.* **2000**, *32*, 435.

(6) Curran, H. J.; Fischer, S. L.; Dryer, F. L. *Int. J. Chem. Kinet.* **2000**, *32*, 741.

(7) Sehested, J.; Sehested, K.; Platz, J.; Egsgaard, H.; Nielsen, O. J. *Int. J. Chem. Kinet.* **1997**, *29*, 627.
(8) Dagaut, P.; Boettner, J. C.; Cathonnet, M. Proceedings of the Twenty-Sixth International Symposium on Combustion, Napoli, Italy, 1996.
(9) Loucks, L. F.; Laidler, K. J. *Can. J. Chem.* **1967**, *45*, 2767
(10) Benson, S. W.; Jain, D. V. S. *J. Chem. Phys.* **1959**, *31*, 1008.
(11) Marcus, R. A.; Darwent, B. D.; Steacie, E. W. R. *J. Chem. Phys.* **1948**, 987.
(12) Hase, W. *Acc. Chem. Res.* **1998**, *31*, 659.
(13) Truhlar, D. G.; Garrett, B. C.; Klippenstein, S. J. *J. Phys. Chem.* **1996**, *100*, 12771.
(14) Truhlar, D. G.; Gordon, M. S. *Science* **1990**, *249*, 491.
(15) Truong, N. T.; Truhlar, D. G. *J. Chem. Phys.* **1990**, *93*, 1761.
(16) Lynch, B. J.; Fast, P. L.; Harris, M.; Truhlar, D. G. *J. Phys. Chem. A* **2000**, *104*, 4811.
(17) Chuang, Y. Y.; Coitino, E. L.; Truhlar, D. G. *J. Phys. Chem. A* **2000**, *104*, 446.
(18) Pople, J. A.; Head-Gordon, M.; Raghavachari, K. *J. Chem. Phys.* **1987**, *87*, 5968.
(19) Lynch, B. J.; Truhlar, D. G. *J. Phys. Chem. A* **2001**, *105*, 2936.
(20) Parthiban, S.; Oliveira, G. D.; Martin, J. M. L. *J. Phys. Chem. A* **2001**, *105*, 895.
(21) Gonzalez, C.; Schlegel, H. B. *J. Chem. Phys.* **1989**, *90*, 2154.
(22) Woon, D. E.; Dunning, T. H. *J. Chem. Phys.* **1993**, *98*, 1358.
(23) Frisch, M. J.; Trucks, G. W.; Schlegel, H. B.; Scuseria, G. E.; Robb, M. A.; Cheeseman, J. R.; Zakrzewski, V. G.; Montgomery, J. A., Jr.; Stratmann, R. E.; Burant, J. C.; Dapprich, S.; Millam, J. M.; Daniels, A. D.; Kudin, K. N.; Strain, M. C.; Farkas, O.; Tomasi, J.; Barone, V.; Cossi, M.; Cammi, R.; Mennucci, B.; Pomelli, C.; Adamo, C.; Clifford, S.; Ochterski, J.; Petersson, G. A.; Ayala, P. Y.; Cui, Q.; Morokuma, K.; Malick, D. K.; Rabuck, A. D.; Raghavachari, K.; Foresman, J. B.; Cioslowski, J.; Ortiz, J. V.; Stefanov, B. B.; Liu, G.; Liashenko, A.; Piskorz, P.; Komaromi, I.; Gomperts, R.; Martin, R. L.; Fox, D. J.; Keith, T.; Al-Laham, M. A.; Peng, C. Y.; Nanayakkara, A.; Gonzalez, C.; Challacombe, M.; Gill, P. M. W.; Johnson, B. G.; Chen, W.; Wong, M. W.; Andres, J. L.; Head-Gordon, M.; Replogle, E. S.; Pople, J. A. *Gaussian 98*; Gaussian, Inc.: Pittsburgh, PA, 1998.
(24) Truhlar, D. G.; Garrett, B. C. *Annu. Rev. Phys. Chem.* **1984**, *35*, 159.
(25) Truong, T. N. *J. Chem. Phys.* **1994**, *100*, 8014.
(26) Truhlar, D. G.; Fast, P. L. *J. Chem. Phys.* **1998**, *109*, 3721.
(27) Garrett, B. C.; Truhlar, D. G. *J. Phys. Chem.* **1979**, *83*, 1079.
(28) Isaacson, A. D.; Sund, M. T.; Rai, S. N.; Truhlar, D. G. *J. Chem. Phys.* **1985**, *82*, 1338.
(29) Zhang, S.; Truong, T. N. *VKLab*, version 1.0; University of Utah: Salt Lake City, UT, 2001.
(30) Caralp, F.; Devolder, P.; Fittschen, C.; Gomez, N.; Hippler, H.; Mereau, R.; Rayez, M. T.; Striebel, F.; Viskolcz, B. *Phys. Chem. Chem. Phys.* **1999**, *1*, 2935
(31) Petraco, N. D. K.; Allen, W. D.; Schaefer, H. F., III. *J. Chem. Phys.* **2002**, *116*, 10229.
(32) Clabo, D. A.; Allen, W. D.; Reminton, R. B.; Yamaguchi, Y.; Schaefer, H. F., III. *Chem. Phys.* **1988**, *123*, 187.
(33) Duncan, J. L. *Mol. Phys.* **1974**, *28*, 1177.
(34) Shimanouchi, T. *Tables of Molecular Vibrational Frequencies Consolidated*; National Bureau of Standards, 1972; Vol. 1.
(35) Ira, N. L. *Molecular Spectroscopy*; Wiley: New York, 1975.
(36) Jacox, M. E. *J. Mol. Spectrosc.* **1977**, *106*, 272.
(37) Hadrich, S.; Hefter, S.; Pfelzer, B.; Doerk, T.; Jauernik, P.; Uhlenbusch, J. *Chem. Phys. Lett.* **1996**, *256*, 83.
(38) Tam, S.; Macler, M.; Fajardo, M. E. *J. Chem. Phys.* **1997**, *106*, 8955.
(39) Chase, M. W., Jr. *NIST-JANAF Themochemical Tables*, 4 ed.; Journal of Physical and Chemical Reference Data, Monograph No. 9; American Chemical Society: Washington, DC, 1998; p 1.
(40) Truhlar, D. G.; Kuppermann, A. *J. Am. Chem. Soc.* **1971**, *93*, 1840.
(41) Garrett, B. C.; Truhlar, D. G. *J. Phys. Chem.* **1979**, *83*, 1052.